Earth and Planetary Science Letters 296 (2010) 144–152

Contents lists available at ScienceDirect

Earth and Planetary Science Letters

journal homepage: www.elsevier.com/locate/epsl

An efficient mechanism to avert frictional melts during seismic ruptures

Andrea Bizzarri *

Istituto Nazionale di Geofisica e Vulcanologia, Sezione di Bologna, Via Donato Creti, 12, 40128 Bologna, Italy

ARTICLE INFO

Article history:
Received 16 December 2009
Received in revised form 23 April 2010
Accepted 14 May 2010
Available online 9 June 2010

Editor: R.D. van der Hilst

Keywords:
earthquake dynamics
frictional heat
melting
constitutive equation
computational seismology

ABSTRACT

We consider the spatio-temporal evolution of temperature due to frictional heating caused by the spontaneous propagation of 3-D dynamic seismic ruptures on planar faults. In our numerical experiments, which characterize typical crustal earthquakes, we assume that fault friction is controlled by different linear and nonlinear slip-dependent friction laws. In this paper we confirm that a necessary condition to prevent melting is to have a nearly complete breakdown stress drop. Our simulations, which employ a nonlinear slip-dependent governing equation recently inferred from laboratory experiments by Sone and Shimamoto (2009), reproduce such a dramatic fault weakening and represent a plausible explanation for the prevention of melting during earthquake ruptures. We also demonstrate that low friction alone, although necessary, is not a sufficient condition to avert melts; the linear (or classical) slip-weakening (SW) law would produce melting, even assuming the same lengthscales and frictional levels. To avoid melting with linear SW law we have to impose a specific value of the SW distance. This reveals the prominent role of the time evolution of traction within the cohesive zone, where the stress release is realized, and of the value of the fracture energy density.

1. Introduction

The apparent scarcity of glassy-like pseudotachylytes (Sibson, 2003) has contributed to development of a vigorous debate in the fault mechanics community regarding the occurrence of frictional melting during dynamic earthquake propagation (see Kirkpatrick et al., 2009 and references therein). It is well known that a large number of chemico-physical processes can take place during a faulting episode (see Bizzarri , 2009b for a review). In particular, some thermally-activated phenomena have been proposed as possible explanations for the apparent lack of melting, all of them having in common the dramatic reduction of fault friction (weakening) during the coseismic phase of an earthquake failure (Sibson, 1973).

One of these candidate mechanisms is thermal pressurization of pore fluids (e.g., Andrews, 2002; Sibson, 2003; Rice, 2006 among many others) whereby pore fluids can become pressurized due to frictional heating and reduce the effective normal stress on a fault; nevertheless, 3-D numerical simulations of Bizzarri and Cocco (2006a, 2006b) showed that the significant stress releases caused by thermal pressurization are counterbalanced by an enhanced instability. The net effect is that the generated temperature exceeds the melting point when the slipping (or shear) zone of width $2w$, where slip is concentrated (Ben-Zion and Sammis, 2003; Sibson, 2003), is sufficiently thin, i.e., smaller than few mm in thickness.

Another physical mechanism often considered to explain the apparent rarity of bulk friction melts is flash heating of micro-asperity contacts (e.g., Noda et al., 2009 and references therein); however, Bizzarri (2009a) demonstrated that, even if large stress releases due to flash heating are realized, the supershear rupture regime is favored and values of fault slip velocity are very high (~60 m/s at maximum). Consequently the resulting temperature rise on the fault is expected to induce bulk melting.

The aim of the present paper is to explore, through numerical experiments, whether a new, laboratory-derived friction law, recently inferred by Sone and Shimamoto (2009; hereafter referred to as SS09), represents an efficient and plausible physical mechanism to avert melting during dynamic ruptures.

2. Numerical solution of elasto-dynamic problem

Here we consider the fully dynamic propagation of an earthquake rupture, spontaneously spreading over a strike-slip fault of finite width embedded in a Hookean isotropic medium initially at mechanical equilibrium. The solution of this kind of problem can be only obtained numerically; this is accomplished via the finite-difference, conventional-grid (FDCG) code described in Bizzarri and Cocco (2005). Fault strength is specified through the introduction of a governing equation, which controls the traction evolution. In this paper we assume that the shear traction τ, is described by the

* Tel.: +39 051 4151432; fax: +39 051 4151499.
E-mail address: bizzarri@bo.ingv.it.

0012-821X/$ – see front matter © 2010 Elsevier B.V. All rights reserved.
doi:10.1016/j.epsl.2010.05.012

following nonlinear slip-dependent governing model, recently inferred from laboratory experiments by SS09 and references cited therein:

$$\tau = \left\{\mu^{ss}(v) + \left[F(u)\mu_i - \mu^{ss}(v)\right]e^{\frac{\gamma u}{d}}\right\}\sigma_n^{\text{eff}} \tag{1}$$

where $\mu^{ss}(v) = \mu^{ss}(0)e^{-\frac{v}{v_{ss}}}$, $F(u) = a_{ss} + (1-a_{ss})e^{\frac{\gamma u}{u_h}}$ and γ is a dimensionless constant ($\gamma \equiv \ln(0.05)$; note that $\gamma<0$ and therefore τ does not diverge for arbitrarily large slips). Model (1) represents a slip- and velocity-weakening friction law, since τ depends explicitly on fault slip u, and its time derivative v (v_{SS} is a cutoff velocity and μ_i is the friction coefficient at $t=0$). Eq. (1) has been derived by fitting data obtained by SS09 in high-velocity frictional experiments (at both constant and variable velocities) using natural fault gouge samples collected from the Chelungpu fault, Taiwan. In addition to the high sliding velocity realized during the experiments, up to 2 m/s, the novelty of the experiments is represented by the fact that the imposed velocity is varied through time, in an effort to simulate accelerating and decelerating fault motion associated with dynamic rupture.

Representative behavior of the fault strength in the case of the adopted constitutive model (1) is shown in Fig. 1, in which we plot the evolution of the function of two variables $\tau = \tau(u,v)$ as expressed by Eq. (1) and normalized by σ_n^{eff} (namely, we represent the friction coefficient, $\mu = \tau/\sigma_n^{\text{eff}}$). The plot is obtained by assuming the parameters listed in Table 1. Even for moderate fault slip velocities, Fig. 1 shows that the friction coefficient is extremely low for $u \geq 1$ m; for example, for the adopted parameters, when $v = 5$ m/s we have $\mu = 0.04$ for $u = 1$ m.

In the constitutive model (1) $F(u)$ describes the preparatory phase (basically consisting of micro-cracking) of the imminent macroscopic failure causing the breakdown stress drop, i.e., the decrease of traction from its peak value down to the residual level. This preparatory stage can be associated with the so-called direct effect within the framework of rate- and state-dependent friction laws (e.g., Dieterich, 1979; Beeler et al., 1994; Ruina, 1983), which initially works against fault weakening (see also Bizzarri and Cocco, 2003). This slip-hardening phase (described by the constitutive parameters α_{SS} and u_h of Eq. (1)) has been documented both in laboratory experiments (Ohnaka and Yamashita, 1989; see also Matsu'ura et al., 1992) and in kinematic inversions of seismic data (Ide and Takeo, 1997). The slip accumulated when the traction reaches its maximum value is determined by the competition between the initial strengthening phase and the subsequent slip- and velocity-weakening phase. The latter stage can be physically interpreted as the abrasion of surface asperities, leading to the decrease of frictional resistance; when the surfaces are soft the slip-weakening proceeds fast and when they are very hard the abrasion rate is very small.

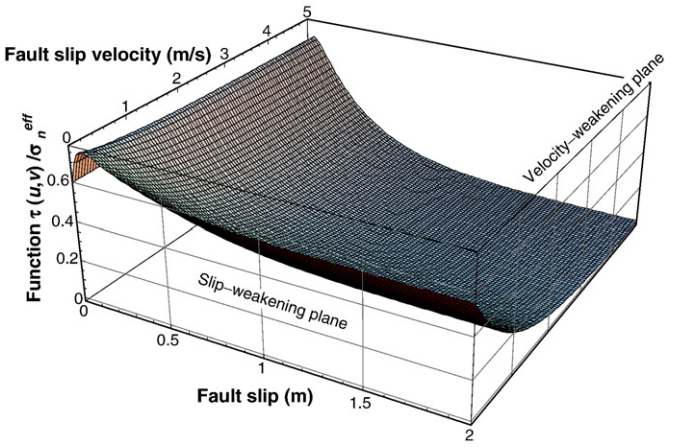

Fig. 1. Evolution of the function $\tau = \tau(u,v)$ expressed by Eq. (1) and normalized by the effective normal stress, plotted for the parameters assumed in the present study (see Table 1).

Table 1
Reference parameters adopted in the present study.

Parameter	Value
Medium and discretization parameters	
Lamé constants, $\lambda = G$	27 GPa
S-wave velocity, v_S	3 km/s
P-wave velocity, v_P	5.196 km/s
Cubic mass density, ρ	2700 kg/m^3
Fault length, L^f	12 km
Fault width, W^f	11.6 km
Spatial grid size, $\Delta x_1 = \Delta x_2 = \Delta x_3 \equiv \Delta x$	8 m
Time step, Δt	4.44×10^{-4} s
Final computed time, t_{end}	1.1 s[a]
Courant–Friedrichs–Lewy ratio, $\omega_{\text{CFL}} = v_S \Delta t / \Delta x$	0.1665
Critical frequency for spatial grid dispersion, $f_{\text{acc}}^{(s)} = v_S/(6\Delta x)$	62.5 Hz
Coordinates of the hypocenter, (x_1^H, x_3^H)	(5.992,7) km
Reference constitutive parameters of the constitutive model (1)	
Effective normal stress, σ_n^{eff}	120 MPa
Initial value of friction coefficient, μ_i	0.6[b]
Initial steady-state frictional coefficient, μ^{ss} (0)	0.55
Cutoff velocity, α_{SS}	0.99 m/s
Parameter controlling the slip-hardening, μ_{SS}	1.4
Characteristic slip-hardening distance, u_h	0.1 m
Characteristic slip-weakening distance, d	1 m
Reference thermal parameters	
Initial temperature in the center of the slipping zone, T_0^f	210 °C[c]
Heat capacity for unit volume of the bulk composite, c	3×10^6 J/(m^3 °C)
Thermal diffusivity, χ	1×10^{-6} m^2/s
Slipping zone thickness, $2w$	0.01 m
Parameter ε in Eq. (4)	$\Delta t = 4.44\times10^{-4}$ s[d]

[a] t_{end} ensures that the rupture does not hit the fault boundaries (and therefore no back propagating fronts arising from the free surface interaction came back into the model). We do not introduce any healing mechanism in the simulations presented here.
[b] At $t=0$ the fault is locked (i.e., $u=0$) and therefore $F(u)=0$. From Eq. (1) we have that, at $t=0$, the traction τ_0 is then expressed as $\mu_i\sigma_n^{\text{eff}}$ (= 72 MPa for our parameters).
[c] A geothermal gradient of 30 °C/km is assumed.
[d] See Bizzarri and Cocco (2006a; their Appendix A for further numerical and analytical details).

Eq. (1) can be regarded as a more general formulation of the classical slip-weakening (SW) law (Ida, 1972; his model 2), which postulates a linear dependence of frictional resistance on fault slip:

$$\tau = \begin{cases} \tau_u - \left(\tau_u - \tau_f\right)\dfrac{u}{d_0}, & u < d_0 \\ \tau_f, & u \geq d_0 \end{cases} \tag{2}$$

Governing model (2) basically describes the breakdown stress drop process over a finite time interval (i.e., not instantaneous) and has been derived from a theoretical basis. In Eq. (1) σ_n^{eff} is the effective normal stress, assumed to be constant through time in the first part of this work (we will discuss time variations of σ_n^{eff} in Section 6). The parameter d, which is the counterpart of d_0 in Eq. (2), is the scale distance characterizing the breakdown phase, during which the traction degrades from its maximum value down to its residual level. These maximum and residual frictional levels are explicitly (a priori) given in the framework of the linear SW model (τ_u and τ_f in Eq. (2), respectively), while they depend on rupture dynamics in the constitutive model (1). An analytical estimate of the equivalent stress levels (as defined in Cocco and Bizzarri, 2002) in the case of a spontaneously spreading rupture obeying model (1) is derived in Appendix A.

In the remainder of the paper we will consider the frictional heat developed during sliding, which is given by the solution of the Fourier

conduction equation. At a generic fault node (x_1,x_3) at time t the temperature is given by:

$$T^{\mathrm{f}}(x_1,x_3,t) = T_0^{\mathrm{f}} + \frac{1}{2cw}\int_0^{t-\varepsilon} dt' \operatorname{erf}\left(\frac{w}{2\sqrt{\chi(t-t')}}\right)\tau\left(x_1,x_3,t'\right)v\left(x_1,x_3,t'\right) \tag{3}$$

where T_0^{f} is the initial temperature in the center of a fault structure having a slipping zone which is $2w$ in width (Sleep, 1997; Ben-Zion and Sammis, 2003), c is the heat capacity for unit volume of the bulk composite, χ is the thermal diffusivity, erf(.) is the error function and ε is an arbitrarily small positive real number (see Bizzarri and Cocco, 2006a for numerical and analytical details).

3. Adopted parameters

The parameters adopted in this paper are tabulated in Table 1; they are representative of a typical crustal earthquake occurring at the depth of 7 km. The constitutive parameters of constitutive model (1) are those inferred by SS09, except for d, which depends on the applied normal stress (SS09). In fact, the normal stresses used in the SS09 experiments are much lower than those expected at seismogenic depths; therefore we have extrapolated the value of d for $\sigma_n^{\mathrm{eff}} = 120$ MPa by fitting the laboratory data of SS09 with the power law function $d = a(\sigma_n^{\mathrm{eff}})^{-b}$ (with $a = 3.26\times10^3$ m Pa^b and $b = 0.43$, when σ_n^{eff} is expressed in Pascal and d in meter). This can be considered as an upper bound on d at seismogenic depths; the SS09 data can be also fitted with the inverse proportionality function $d = c/\sigma_n^{\mathrm{eff}}$ (with $c = 3\times10^6$ m Pa), which gives $d = 5$ cm for $\sigma_n^{\mathrm{eff}} = 120$ MPa. A value of $d = 5$ cm can be considered as a lower bound for the SW distance for the assumed normal load. The value of u_h is expected to decrease slightly with increasing normal stress, but we made the conservative choice to adopt the same value as in SS09.

To better understand the basic features of the model we assume homogeneous properties in the fault zone; this would cause a continuous enlargement of the rupture up to the fault boundaries. Nucleation is obtained by initially forcing the rupture to develop at a prescribed constant speed, as discussed in detail in Bizzarri (2010).

4. How to prevent melting

The comparison of the frictionally generated temperature for ruptures obeying Eqs. (1) and (2) is reported in Fig. 2a and b, respectively. In the case of constitutive model (1) the generated temperature remains well below the bulk melting temperature of the rock, $T_{\mathrm{melt}} = 1500$ °C (Fig. 2a); in contrast, with the linear SW law (2), melting occurs (Fig. 2b). As indicated by the red curve in Fig. 3, slip velocities predicted by model (1) are very large ($v\sim50$ m/s; Fig. 3b), but the breakdown stress drop is nearly complete (i.e., the final value of traction is extremely low; Fig. 3a). As a consequence, the balance between the time histories of slip velocity and fault traction appearing in (3) causes the generated temperature to be too low for melting.

Extreme fault weakening is an intrinsic feature of the governing model (1) and is a necessary condition to avert melting. As already noted above, the limiting velocity in the SS09 laboratory experiments is 2 m/s; we have therefore also considered a special case of model (1) in which the steady-state function $\mu^{ss}(v)$ is held constant at high velocities (namely, $\mu^{ss}(v) = \mu^{ss}(0)e^{-\frac{2}{v_{ss}}}$ for $v \geq 2$ m/s). The results obtained in this case are shown as red dotted lines in Fig. 3; in this configuration the balance between v (with peaks $\sim$36 m/s) and τ ($\tau_f^{\mathrm{eq}}\sim8$ MPa) is such that $T^{\mathrm{f}} > T_{\mathrm{melt}}$, indicating that the value of the friction is not sufficiently low to prevent melting.

An extremely low value of fault traction is a necessary but insufficient condition to avert melting. To prove this claim, we performed a numerical experiment assuming the linear SW model (2) with the same levels of stress as in the simulation with model (1). From Fig. 3a the maximum yield stress $\tau_u^{\mathrm{eq}} = 81.717$ MPa (in excellent agreement with the analytical estimate of 81.722 MPa given by Eq. (A.6)) is realized for $u = u_u = 41.25$ mm (in agreement, given the spatial resolution of the model, with the prediction of Eq. (A.4) of 38.23 mm). Moreover, again from Fig. 3a, we can infer: $\tau_f^{\mathrm{eq}} = 600$ Pa and $d_0^{\mathrm{eq}} = 2$ m. (We emphasize that $u_u < u_h$ and $d_0^{\mathrm{eq}} > d$, in complete agreement with the experimental results of SS09). These values depend slightly on the position on the fault, but can be regarded as representative of the traction behavior over the whole fault surface. By assuming the above-mentioned values ($\tau_u = \tau_u^{\mathrm{eq}}$, $\tau_f = \tau_f^{\mathrm{eq}}$ and $d = d_0^{\mathrm{eq}}$), model (2) produces the results plotted with black lines in Fig. 3. The initial conditions are identical in the two models (as are the thermal parameters; Table 1). We note that the final traction is exactly the same in both models; moreover, peaks in v are even lower with the linear SW law than in the case of model (1). However, the traction evolution within the cohesive zone is rather different in the two

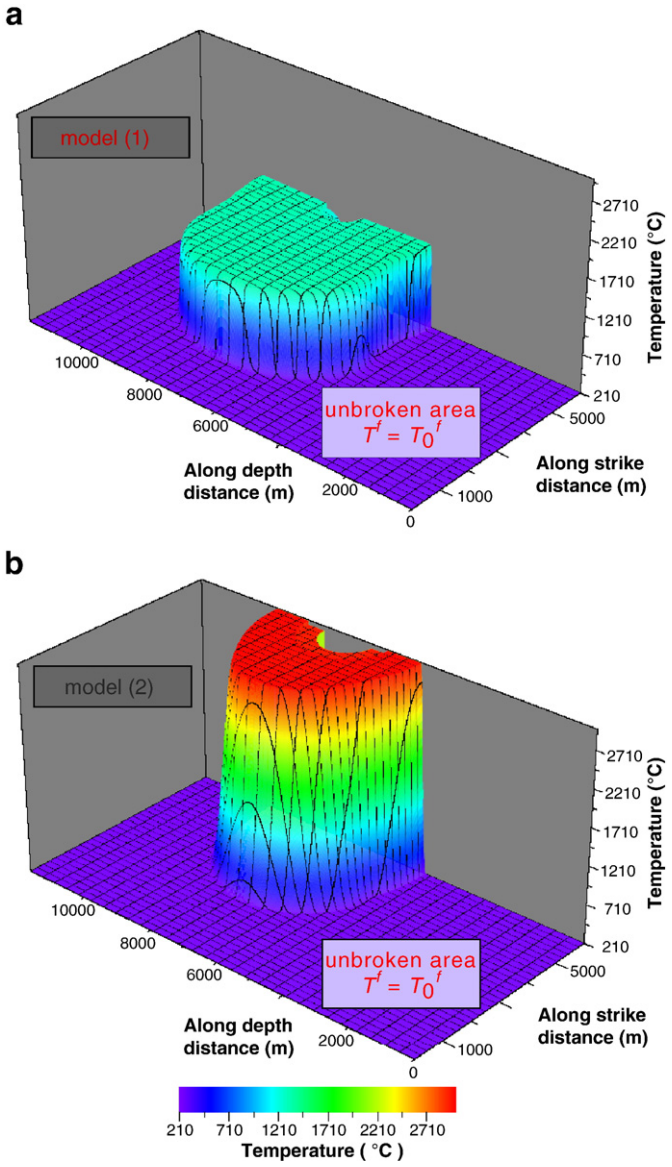

Fig. 2. Spatial distribution of the developed temperature, $T^{\mathrm{f}}(x_1,x_3)$, as given by Eq. (3) at the end of the numerical experiments. (a) Case of constitutive model (1). (b) Case of linear SW law (Eq. (2)). Due to the symmetry exploitation in the strike direction (see Bizzarri, 2009a for technical details), only one half of the fault plane in the strike direction is reported.

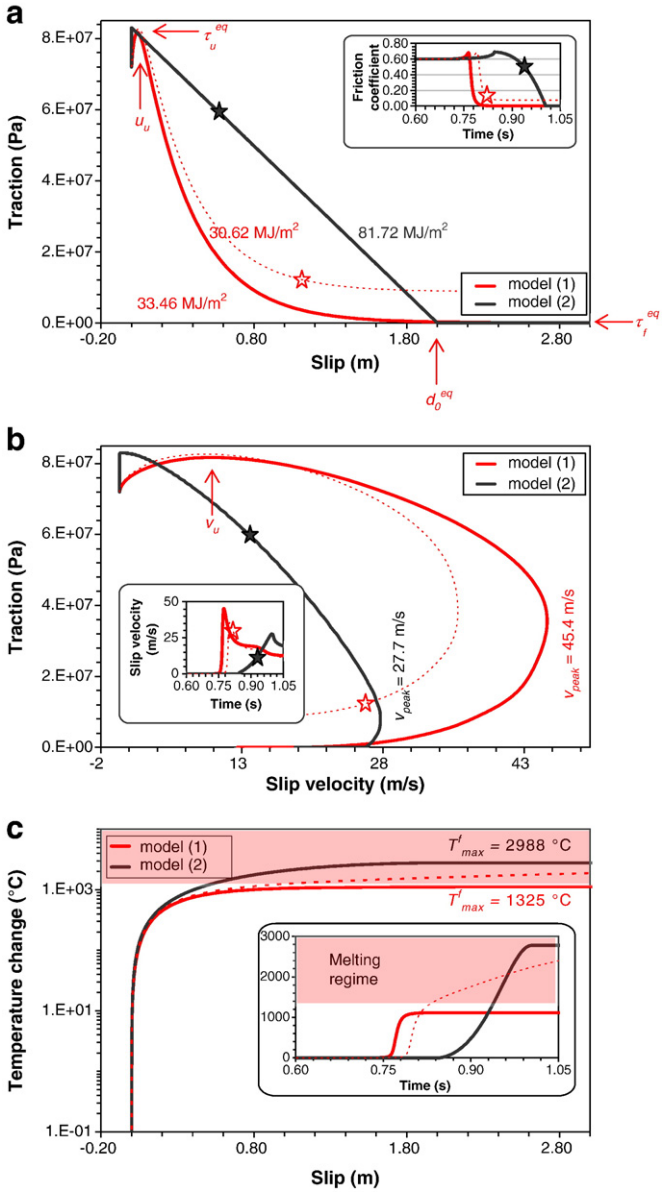

Fig. 3. Comparison between solutions obtained with constitutive models (1) and (2) (red and black curves, respectively). (a) Traction vs. slip, with inset reporting the time evolution of the friction coefficient. (b) Phase diagram, with inset showing the slip velocity time histories. (c) Temperature change, $\Delta T^f = T^f - T_0^f$, as a function of slip, with inset reporting ΔT^f vs. time. In all panels, which refer to a fault point at hypocentral depth and located at a strike distance from the hypocenter of 3 km, the red dotted curve pertains to model (1) with a high-speed cutoff in the function $\mu^{ss}(v)$ (see text for details). Stars show when melting occurs. For each model the value of the resulting fracture energy density, E_G, is indicated ($E_G = \int_0^d (\tau - \tau_{res})du$, where τ_{res} is the level of friction after the completion of the breakdown phase; Bizzarri, in press).

models (see Fig. 3a), as well as the fracture energy density, E_G, which physically represents the work done against the resistance to fault extension at the rupture tip (or, equivalently, as the amount of energy necessary to maintain an ongoing propagating rupture; e.g., Bizzarri, in press). Later on the paper we will discuss the case in which both models (1) and (2) has the same E_G. The different traction history, entering in the time convolution of Eq. (3), causes T_{melt} to be exceeded in the case of the linear SW law ($T^f \sim 3000$ °C at the end of the numerical simulation; Figs. 2b and 3c). Note that melting occurs during the breakdown phase (see the star in Fig. 3a), well above the kinetic level of friction.

It is apparent from Fig. 3b that, within the time window explored here, the fault does not heal after weakening in the two governing models; this is not surprising in the case of the linear SW law, which does not contain any mechanism for rapid strengthening. In all cases the temperature saturates (Fig. 3c) at large slips (and times) as a consequence of the very low and constant value of the shear traction.

5. The importance of traction history within the cohesive zone

As discussed previously, extreme fault weakening is necessary but an insufficient condition to prevent frictional melts. We performed additional numerical experiments by assuming smaller values of d_0 in model (2); these cause a reduction of E_G with respect to the large value obtained in previous SW simulation (see Fig. 3). From the results reported in Fig. 4 we can see that even with $d_0 = 1$ m (which is markedly smaller than the value of d_0^{eq} resulting from model (1)) melting is occurring. Even if the slip velocity function is basically the same (except for a temporal shift, see inset in Fig. 4b) and the residual level of friction is attained at even lower values of slip in the case of the linear SW model (black curve in Fig. 4a), the exponential decay of traction in model (1) prevents melting, while the linear decay in model (2) does not. By further decreasing d_0 ($d_0 = 0.5$ m) it is possible to avert melting with the linear SW equation (grey curves in Fig. 4). However, we emphasize that in the case of linear SW law we have to find in parameter space (and then to impose) optimal values of the residual friction and the characteristic SW distance which prevent

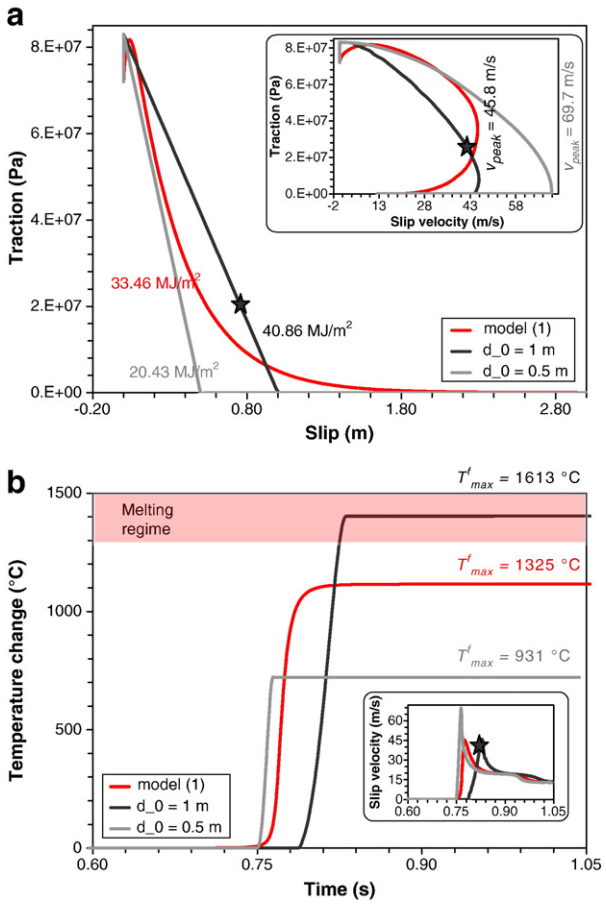

Fig. 4. Results for linear SW law (2) with different characteristic distances d_0 (the values are indicated in the legend). (a) Traction vs. slip, with inset reporting the phase diagram. (b) Time evolution of ΔT^f with inset showing the slip velocity history. Results all plotted for the same location as in Fig. 3. For comparison red curves in all panels show the results for model (1) (the same as in Fig. 3). The star shows when melting occurs. Values of E_G are indicated.

melting. In the governing model (1) the low value of friction is a product of the model itself and we do not have to make any arbitrary choice.

Finally, we note that all models with linear SW friction have a low value of the strength parameter ($S = \frac{\tau_u - \tau_0}{\tau_0 - \tau_f} = 0.13$; Das and Aki, 1977) and peak slip velocity is attained when friction reaches the final, kinetic level (inset panel in Fig. 4a), in agreement with the results of Tinti et al. (2004). In contrast, the constitutive model (1) predicts that the peak in v is reached when the traction is higher than τ_f^{eq} and consequently slip is smaller than d_0^{eq}. This further complicates attempts to retrieve the SW distance from the slip velocity history, as some authors have proposed (e.g., Fukuyama et al., 2003).

A friction law similar to model (1) has been proposed by Ohnaka and Yamashita (1989; see also Abercrombie and Rice, 2005) by fitting data from laboratory experiments for a mode II crack growing along a preexisting fault in a granite sample:

$$\tau = \left[\left(\mu_i \sigma_n^{eff} - \tau_f\right)\left(1 + \alpha_{OY} \ln\left(1 + \frac{u}{\beta_{OY}}\right)\right) e^{-\frac{u}{d'}} + \tau_f\right] \quad (4)$$

where α_{OY} and β_{OY} are the governing parameters accounting for the slip-hardening phase and d' is a characteristic distance controlling the weakening stage. In fact, the exponential weakening is not a new concept (see Lachenbruch, 1980); indeed the terms inside the second round brackets in Eq. (4) recall the theoretical derivation of Matsu'ura et al. (1992), which reads: $e^{\frac{u}{d'}} e^{-\frac{u}{d'}}$. Following Bizzarri and Belardinelli (2008; their Appendix A), by adopting $d' = 0.35$ m, $\alpha_{OY} = 0.2$ and $\beta_{OY} = 14$ mm we obtain a SW curve which fits the red line in Fig. 3a. The corresponding results are reported in Fig. 5.

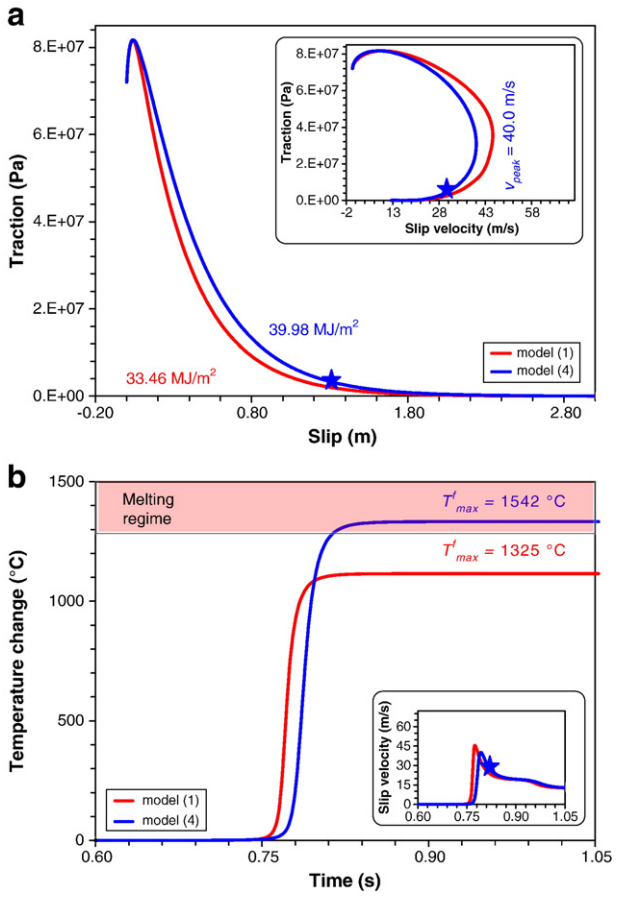

Fig. 5. The same as in Fig. 4, but now for the nonlinear slip-dependent model (4) (blue curves).

Although the levels of stress are identical in the two cases – and attained for the same values of slip, as desired – the weakening process is slightly different in the two models; this is not surprising, given the fact that in model (4) there is no explicit dependence of friction on sliding velocity, as in model (1). Correspondingly, the fracture energy density is slightly different in two simulations, but the difference is smaller than in previous cases. Even if the slip velocity is smaller in Eq. (4) (insets in Fig. 5a and b), the melting temperature is reached and slightly exceeded in model (4) (Fig. 5b). However, the generated temperature is smaller than that obtained with the linear SW law (see Section 3), indicating that an exponential weakening tends to prevent melting. Moreover, this simulation further demonstrates that both the final level of friction and the behavior of τ within the cohesive zone are of primary importance in the discrimination between melting and non-melting regimes.

We finally remark that in model (4) the frictional level of friction has to be assigned a priori (as in model (2)) and it is not a part of solution as in Eq. (1).

6. Effects of the normal stress

All previous results have been obtained by assuming $\sigma_n^{eff} = 120$ MPa. If we assume a fluid-saturated fault zone, then the effective normal stress would change through time accordingly to the following equation (see Bizzarri and Cocco (2006a) for details):

$$\sigma_n^{eff} = \sigma_n - p_{fluid}^f(x_1, x_3, t) = \sigma_n - p_{fluid_0}^f - \frac{\alpha_{fluid}}{2cw\beta_{fluid}} \quad (5)$$
$$\times \int_0^{t-\varepsilon} dt' \left\{ -\frac{\chi}{\omega - \chi} \mathrm{erf}\left(\frac{w}{2\sqrt{\chi(t-t')}}\right) + \frac{\omega}{\omega - \chi} \mathrm{erf}\left(\frac{w}{2\sqrt{\omega(t-t')}}\right) \right\}$$
$$\times \tau\left(x_1, x_3, t'\right) v\left(x_1, x_3, t'\right)$$

where σ_n is the tectonic (lithostatic) load, $p_{fluid_0}^f$ is the initial fluid pressure distribution, ω is the hydraulic diffusivity ($\omega \equiv \frac{k}{\eta_{fluid}\beta_{fluid}\Phi}$, being k the permeability of the medium, β_{fluid} the compressibility coefficient of the fluid and η_{fluid} its dynamic viscosity), and α_{fluid} is the coefficient of thermal expansion. Eq. (5) is the solution of the thermal pressurization problem when a constant porosity Φ is assumed (Bizzarri and Cocco, 2006b discuss the more general case, where dilatancy is accounted for). Results for a fault obeying constitutive model (1) with the addition of the thermal pressurization is reported by dashed red and blue curves in Fig. 6. Even assuming a low hydraulic diffusivity ($\omega = 0.0001$ m^2/s for blue curves in Fig. 6) the behavior is nearly identical to the reference case, where p_{fluid} does not change (solid red curves in Fig. 6). Thermal pressurization slightly decreases the fault friction (now $\tau_f^{eq} = 500$ Pa, instead of 600 Pa), but the dramatic weakening caused by the constitutive model (1) is paramount. Correspondingly, the introduction of the thermal pressurization produce small effects on temperature change (Fig. 6b); the major outcome is that also with thermal pressurization, the dynamic evolution of the fault is such that melting is averted.

We have also considered different scenarios, having completely different values of normal stress. The value of σ_n^{eff} assumed above can be regarded as a representative value of the normal stress over the whole fault. Since slip occurs also near the free surface we have also considered a rupture propagating on dry fault which nucleates at a depth of 2.5 km (in this case $\sigma_n^{eff} = \sigma_n = 66$ MPa and $T_0^f = 75$ °C). Also in this case melting does not occur (see grey curves in Fig. 6). On the contrary, by assuming a dry fault and maintaining the hypocentral depth of 7 km (in this case $\sigma_n^{eff} = \sigma_n = 66$ MPa and $T_0^f = 210$ °C) the traction evolution causes melting (solid black curves in Fig. 6). However, if we assume the same value of initial shear stress as that of

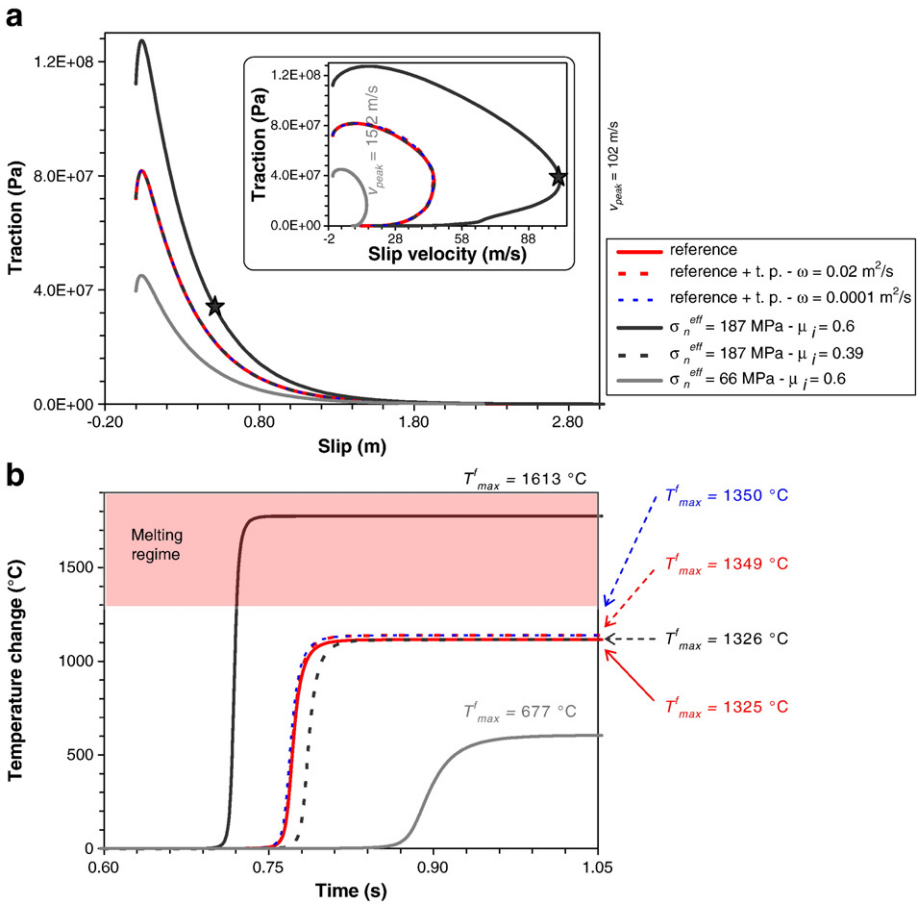

Fig. 6. Effects of the variation of the normal stress for the constitutive model (1). Solid red curves are the reference case (the same as in Fig. 3), while dashed red and blue curves assume the thermal pressurization of pore fluids (Eq. (5), with $\sigma_n = 185$ MPa, $p_{\text{fluid}_0}^{\text{f}} = 65$ MPa, $\alpha_{\text{fluid}} = 1.5\times10^{-3}$ °C^{-1}, $\beta_{\text{fluid}} = 1\times10^{-9}$ Pa^{-1}, $\eta_{\text{fluid}} = 1\times10^{-4}$ Pa s, $\Phi = 0.025$ and $k = 5\times10^{-17}$ m^2 (so that $\omega = 0.02$ m^2/s; dashed red curves) or $k = 2.5\times10^{-19}$ m^2 (so that $\omega = 0.0001$ m^2/s; dashed blue curves). The other parameters are the same as in Table 1). Black curves refer to a dry fault, so that $\sigma_n^{\text{eff}} = \sigma_n = 185$ MPa. Grey curves refer to dry fault with hypocentral depth equal to 2.5 km (so that $T_0^{\text{f}} = 75$ °C; in this case melting regime corresponds to a value of temperature change of 1425 °C). (a) Traction vs. slip, with phase portrait in the inset. (b) Time evolution of ΔT^{f}.

the reference case (so that $\mu_i = 0.39$; dashed black curves in Fig. 6) melting is averted.

7. Discussion and conclusions

In the present paper we calculated the temperature evolution caused by frictional heating, during the spontaneous propagation of a fully dynamic, 3-D rupture on a strike-slip fault, subject to different types of slip-dependent friction laws. The temperature as defined in Eq. (3) is calculated on a mathematical fault plane, located in the center of a slipping zone $2w$ wide (e.g., Chester and Chester, 1998), which is assumed to be representative of the macroscopic behavior of the whole fault zone thickness.

Previous theoretical and numerical studies showed that melting of rocks occurs in seismogenic fault structures with highly localized shear (Fialko, 2004; Nielsen et al., 2008; Rempel and Rice, 2006). The incorporation into fully dynamic models of different physical mechanisms which prescribe a significant reduction in fault traction (such as thermal pressurization of pore fluids, Bizzarri and Cocco, 2006a, 2006b, and flash heating of micro-asperity contacts, Bizzarri, 2009a) causes an enhanced instability, a transition to supershear regimes, but finally do not avert melting.

An outcome of this paper is that a nonlinear slip-dependent governing model, derived experimentally (Sone and Shimamoto, 2009; SS09; see also Han et al., 2010), can be regarded as a possible mechanism to maintain the fault temperature below the melting point (Figs. 2a and 3c). This constitutive model has an empirical origin (it fits laboratory data); although it captures complicated features not described by the simple, linear slip-weakening (SW) law (model (2)), it is a phenomenological description of the frictional behavior at high speeds. The formulation of the physical basis of this constitutive model is beyond the goals of the present study; here we have explored, through accurate numerical simulations, the prominent features of a spontaneous, dynamic earthquake rupture governed by such a rheology.

Our numerical experiments with unbounded slip confirm that a necessary condition to avert melting is a low value of the residual stress level. We found here that the value of the frictional coefficient after the stress release ($\mu \ll 0.1$; Fig. 3a) is dramatically reduced compared with that pertaining to low slip rates ($0.6 < \mu < 0.8$; Byerlee, 1978), in agreement with the results of Han et al. (2010) (see also Hirose and Bystricky, 2007).

Although necessary, a low kinetic friction alone is not a sufficient condition to avert melting; a corresponding linear SW model, with the same constitutive parameters as for the nonlinear SW model, produces melting of rocks (Fig. 2b), despite the fact that the seismic moment is nearly 54% smaller ($M_0 = 1.49\times10^{18}$ Nm) for the linear SW model than for the nonlinear governing model (1) ($M_0 = 2.77\times10^{18}$ Nm).

Numerical experiments with the nonlinear slip-dependent law proposed by Ohnaka and Yamashita (1989) further corroborate that the weakening behavior plays a fundamental role in controlling the amount of frictional heat; although the governing parameters are equivalent (Fig. 5a), the different traction decrease in model (4)

causes melting, in contrast to the governing model (1) (Fig. 5b). The dynamic response of the fault, as well as the fracture energy density, E_G, is very similar in the two models (Fig. 5a), and we cannot exclude that an ad hoc tuning of the constitutive parameters in Eq. (4), leading to the same E_G, will cause a temperature evolution close to that obtained with the SS09 law. This indicates that an exponential decay of friction during weakening (also corroborated by the results of Abercrombie and Rice, 2005) prevents melting.

The characteristic SW distance is not very well constrained seismically because of the band-limitedness; indeed Guatteri and Spudich (2000) demonstrate that only E_G can be stably determined from strong motion data. The fracture energy density is known to control the rupture dynamics (Bizzarri, in press and references therein) and it is therefore one of the most important quantities in earthquake source physics. With the linear SW model (2), assuming the values of peak and residual stress resulting from model (1) (see Fig. 3), a value of $d_0 = 0.82$ m would give the same fracture energy as in model (1). (In this case the two constitutive models are also comparable energetically. We also note that the value of the resulting E_G is in agreement with seismological inferences; e.g., Mai et al., 2006). From Fig. 7 we see that also in this special case the linear SW does not produce melting, indicating that the value of the fracture energy density is also important to discriminate between melting and non-melting regimes.

However, we emphasize that, while in the case of the linear SW law (2) and Ohnaka and Yamashita's law (4) we have to impose a very low value of residual friction (as well as an appropriate value of the characteristic SW distance) as an input parameter in the case of model (1) we do not make any such arbitrary choice, because the constitutive model inherently produces such a low value of friction, essentially controlled by the fault dynamics.

In our numerical experiments we have found that the nearly complete breakdown stress drop does not cause reverse slip. Moreover, in our models we have obtained very high fault slip velocities (~50 m/s). There is no direct evidence of slip velocities this high for real earthquakes, but we emphasize that a brief period of high slip velocity would not be observable in a waveform inversion of ground motions like those of Hartzell and Heaton (1983) and others, owing to the use of low-pass filtered data.

All the simulations presented in this work represent a crack-like propagation. By including some mechanisms to simulate the stopping phase and the consequent healing (e.g., by introducing frictional heterogeneities), the governing model (1) is also able to reproduce a re-strengthening stage, during which the frictional resistance increases for decreasing fault slip velocity. This would potentially produce a temperature increase, basically due to the increase in τ. For the parameters adopted here we found that if the re-strengthening occurs in 0.05 s the fault temperature remains below T_{melt}. On the contrary, if the re-strengthening stage is very slow, it might happen that melting occur.

We suggest that new laboratory experiments exploring very high sliding velocities (and hopefully normal loads comparable to those expected at relevant depths) can illuminate the frictional behavior of real seismic structures; here we have conservatively assumed that the constitutive model (1) is valid for large sliding velocities and normal loads. The laboratory experiments will eventually test the prediction of the nearly complete breakdown stress drops we model. We mention that the model stress drops are greater than the values typically inferred for real earthquakes (e.g., Kanamori and Anderson, 1975), but are compatible with seismological inferences of locally high dynamic stress drops (Spudich et al., 1998). Moreover, dramatic weakening has never been observed in experiments performed at slow slip rates ($v<1$ mm/s), but has been widely reported at $v\sim 1$ m/s (see Mizoguchi et al., 2009 for a review).

For extremely localized shear (i.e., for $2w \ll 10$ mm for the parameters adopted here, in particular for the adopted values of σ_n^{eff}, T_0^f and d_0 (or d')) we found that the constitutive model (1) predicts temperatures significantly lower than those expected with the adoption of the linear SW law (2), but in any case greater than the melting point, regardless of the value of constitutive parameters within the range of their validity (cfr. SS09). In this paper we have shown that, for intermediate degrees of strain localization, a new laboratory-derived friction law can be regarded as a conceivable explanation of the apparent, and widely debated, rarity of pseudotachylytes.

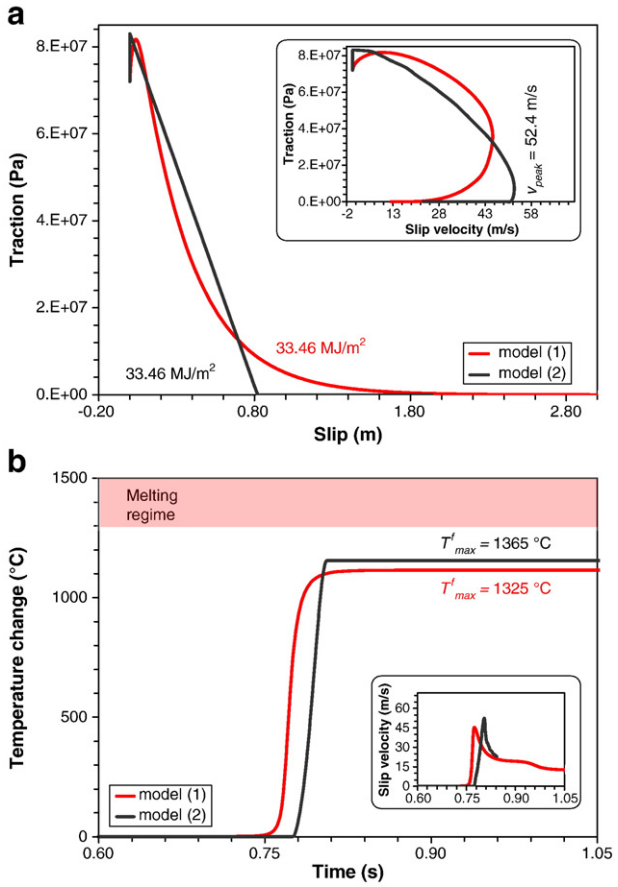

Fig. 7. The same as in Fig. 4, but now model (2) has d_0 such that the fracture energy densities are the same in the two models.

Acknowledgements

I'm indebted to H. Sone and T. Shimamoto for their insightful discussions related to the governing law adopted in this study and to P. Spudich and R. Harris for their comments on a preliminary version of the paper. I also acknowledge the Editor, R. D. van der Hilst and three anonymous referees for the constructive comments that improved the paper.

Appendix A. Analytical estimates of equivalent levels of stress for the constitutive model (1)

In the case of the linear, or classical, slip-weakening model (2) the maximum and kinetic (or residual) levels of friction are prescribed a priori and can be regarded as material properties or input parameters (this makes the implementation of model (2) straightforward, from a computational point of view). On the contrary, as already pointed out in the paper, in the case of the governing model expressed by Eq. (1) these levels of stress cannot be explicitly assigned a priori in a

spontaneous rupture simulation, since they are indeed completely controlled by the fault dynamics. In this appendix we will try to derive some estimation of these quantities analytically.

Following Cocco and Bizzarri (2002) and Bizzarri and Cocco (2003) we denote the above-mentioned frictional levels with symbols τ_u^{eq} and τ_f^{eq}, respectively, indicating the equivalent upper yield stress and equivalent kinetic level, respectively. Specifically, these equivalents are formally expressed as

$$\tau_u^{eq} = \tau(u = u_u, v = v_u) \tag{A.1}$$

and

$$\tau_f^{eq} = \tau\left(u = d_0^{eq}, v = v_f\right), \tag{A.2}$$

respectively. In the previous equations τ represents the analytical function of Eq. (1) expressing the fault traction. In (Eq. A.1) u_u and v_u are the values of fault slip u, and fault slip velocity v, respectively (see also Fig. 3a and b), realized at time $t=t_u$. At t_u the traction attains its absolute maximum (τ_u^{eq}). On the other hand, in Eq. (A.2) d_0^{eq} indicates the amount of cumulative fault slip at which the breakdown stress drop is realized and v_f is the corresponding value of v for that slip. Actually, d_0^{eq} is the equivalent characteristic slip-weakening distance in the terminology of Cocco and Bizzarri (2002) and Bizzarri and Cocco (2003); see also Okubo (1989).

Since the decay of τ for increasing u and v is exponential, it is also useful to define a lower bound estimate, $\breve{\tau}_f^{eq}$, for τ_f^{eq}:

$$\breve{\tau}_f^{eq} = \tau(u \to +\infty, v = v_\infty), \tag{A.3}$$

v_∞ being the value of v at arbitrarily large values of fault slip. Note that $v_\infty = 0$ if the fault heals after the dynamic stress release.

Let us now consider Eq. (A.1). The quantity u_u appearing therein is obtained by solving the equation $\frac{d}{du}\tau(u, v_u) = 0$, which gives:

$$u_u = -\frac{1}{\gamma}u_h\left[\frac{v_u}{v_{SS}} + \ln\left(\frac{\mu_i}{\mu_h}\frac{(d+u_h)(\alpha_{SS}-1)}{\alpha_{SS}\mu_i e^{\frac{v_u}{v_{SS}}} - \mu^{ss}(0)}\right)\right] \tag{A.4}$$

where all the parameters have been defined in Section 2. Notably, it is apparent from Eq. (A.4) that u_u explicitly depends on v_u. If the slip velocity history is imposed, as in the laboratory experiments of SS09 or in kinematic fault models, then u_u can be computed through Eq. (A.4). If the slip velocity history is obtained as a part of the solution, as in spontaneous rupture models, u_u is a priori unknown because v_u is unknown.

It is interesting to note that, in general, u_u does not equal u_h, the constitutive parameter which controls the slip-hardening phase. From Eq. (A.4) we have that the special value of v_u which will satisfy the equality $u_u = u_h$ is expressed as

$$\tilde{v}_u = -v_{SS}\left[1 + \ln\left(\frac{\mu_i}{\mu^{ss}(0)}\frac{e^{-\gamma}u_h\alpha_{SS} - d\alpha_{SS} - u_h\alpha_{SS} + u_h + d}{u_h}\right)\right], \tag{A.5}$$

provided that $e^{-\gamma}u_h\alpha_{SS} - d\alpha_{SS} - u_h\alpha_{SS} + u_h + d > 0$.

Let us now derive an expression for τ_u^{eq} and τ_f^{eq}. By putting the expression of u_u derived in Eq. (A.4) into the definition of τ_u^{eq} (Eq. (A.1)) we can write:

$$\tau_u^{eq} = \mu^{ss}(0)\sigma_n^{eff}e^{-\frac{u_h}{d}\frac{v_u}{v_{SS}}} + \sigma_n^{eff}e^{-\frac{v_h}{d}\frac{v_u}{v_{SS}}}\left(\frac{u_h+d}{u_h}\frac{(\alpha_{SS}-1)\mu_i e^{-\frac{v_u}{v_{SS}}}}{\alpha_{SS}\mu_i - \mu^{ss}(0)e^{-\frac{v_u}{v_{SS}}}}\right)^{-\frac{u_h}{d}} \times \frac{d}{u_h+d}\left(\alpha_{SS}\mu_i - \mu^{ss}(0)e^{-\frac{v_u}{v_{SS}}}\right) \tag{A.6}$$

On the other hand, Eq. (A.3) gives

$$\breve{\tau}_u^{eq} = \mu^{ss}(0)\sigma_n^{eff}e^{-\frac{v_\infty}{v_{SS}}}. \tag{A.7}$$

From Eq. (A.7) we have that, in case of a pulse-like propagation, since $v_\infty = 0, \breve{\tau}_f^{eq} = \mu^{ss}(0)\,\sigma_n^{eff}$. This indicate that the re-strengthening is not complete for the parameters adopted here, in that $\mu^{ss}(0) < \mu_i$ (see Table 1).

Finally, we emphasize that the values of the equivalent stress levels (and therefore the equivalent strength parameter, $S^{eq} = \frac{\tau_u^{eq} - \tau_0}{\tau_0 - \tau_f^{eq}}$) given by Eqs. (A.6) and (A.7) are a priori unknown in a spontaneous fault model. However, these relations can be useful in the case of prescribed sliding velocity (for example, in the setting of a laboratory experiment).

References

Abercrombie, R.E., Rice, J.R., 2005. Can observations of earthquake scaling constrain slip weakening? J. Geophys. Int. 162, 406–424.

Andrews, D.J., 2002. A fault constitutive relation accounting for thermal pressurization of pore fluid. J. Geophys. Res. 105 (B12). doi:10.1029/2002JB001942 2363.

Beeler, N.M., Tullis, T.E., Weeks, J.D., 1994. The roles of time and displacement in the evolution effect in rock friction. Geophys. Res. Lett. 21 (No.18), 1987–1990.

Ben-Zion, Y., Sammis, C.G., 2003. Characterization of fault zones. Pure Appl. Geophys. 160, 677–715.

Bizzarri, A., 2009a. Can flash heating of asperity contacts prevent melting? Geophys. Res. Lett. 36, L11304. doi:10.1029/2009GL037335.

Bizzarri, A., 2009b. What does control earthquake ruptures and dynamic faulting? A review of different competing mechanisms. Pure Appl. Geophys. 166 (Nos. 5–7), 741–776. doi:10.1007/s00024-009-0494-1.

Bizzarri, A., 2010. How to promote earthquake ruptures: different nucleation strategies in a dynamic model with slip-weakening friction. Bull. Seismol. Soc. Am. 100 (No. 3), 923–940. doi:10.1785/0120090179.

Bizzarri, A., in press. On the relations between fracture energy and physical observables in dynamic earthquake models, J. Geophys. Res. doi: 10.1029/2009JB007027.

Bizzarri, A., Belardinelli, M.E., 2008. Modelling instantaneous dynamic triggering in a 3-D fault system: application to the 2000 June South Iceland seismic sequence. Geophys. J. Intl. 173, 906–921. doi:10.1111/j.1365-246X.2008.03765.x.

Bizzarri, A., Cocco, M., 2003. Slip-weakening behavior during the propagation of dynamic ruptures obeying rate- and state-dependent friction laws. J. Geophys. Res. 108 (No. B8). doi:10.1029/2002JB002198 2373.

Bizzarri, A., Cocco, M., 2005. 3D dynamic simulations of spontaneous rupture propagation governed by different constitutive laws with rake rotation allowed. Ann. Geophys. 48 (No. 2), 279–299.

Bizzarri, A., Cocco, M., 2006a. A thermal pressurization model for the spontaneous dynamic rupture propagation on a three-dimensional fault: 1. Methodological approach. J. Geophys. Res. 111. doi:10.1029/2005JB003862 B05303.

Bizzarri, A., Cocco, M., 2006b. A thermal pressurization model for the spontaneous dynamic rupture propagation on a three-dimensional fault: 2. Traction evolution and dynamic parameters. J. Geophys. Res. 111. doi:10.1029/2005JB003864 B05304.

Byerlee, J.D., 1978. Friction of rocks. Pure Appl. Geophys. 116, 615–626.

Chester, F.M., Chester, J.S., 1998. Ultracataclasite structure and friction processes of the Punchbowl fault. San Andreas system, California, Tectonophys, 295, pp. 199–221.

Cocco, M., Bizzarri, A., 2002. On the slip-weakening behavior of rate- and state-dependent constitutive laws. Geophys. Res. Lett. 29. doi:10.1029/2001GL013999.

Das, S., Aki, K., 1977. A numerical study of two-dimensional spontaneous rupture propagation. Geophys. J. R. Astron. Soc. 50, 643–668.

Dieterich, J.H., 1979. Modeling of rock friction: 1. Experimental results and constitutive equations. J. Geophys. Res. 84, 2161–2168.

Fialko, Y.A., 2004. Temperature fields generated by the elastodynamic propagation of shear cracks in the Earth. J. Geophys. Res. 109. doi:10.1029/2003JB002497 B01303.

Fukuyama, E., Mikumo, T., Olsen, K.B., 2003. Estimation of the critical slip-weakening distance: theoretical background. Bull. Seismol. Soc. Am. 93, 1835–1840.

Guatteri, M., Spudich, P., 2000. What can strong motion data tell us about slip-weakening fault friction laws? Bull. Seismol. Soc. Am. 90, 98–116.

Han, R., Hirose, H., Shimamoto, T., 2010. Strong velocity weakening and powder lubrication of simulated carbonate faults at seismic slip rates. J. Geophys. Res. 115, B03412. doi:10.1029/2008JB006136.

Hartzell, S.H., Heaton, T.H., 1983. Inversion of strong ground motion and teleseismic waveform data for the fault rupture history of the 1979 Imperial Valley, California, earthquake. Bull. Seismol. Soc. Am. 73, 1553–1583.

Hirose, T., Bystricky, M., 2007. Extreme dynamic weakening of faults during dehydration by coseismic shear heating. Geophys. Res. Lett. 34. doi:10.1029/2007GL030049 L14311.

Ida, Y., 1972. Cohesive force across the tip of a longitudinal-shear crack and Griffith' s specific surface energy. J. Geophys. Res. 77 (No. 20), 3796–3805.

Ide, S., and M. Takeo, 1997, Determination of constitutive relations of fault slip based on seismic wave analysis, J. Geophys. Res. 102, 27, 379–27, 391.

Kanamori, H., Anderson, D.L., 1975. Theoretical basis of some empirical relations in seismology. Bull. Seismol. Soc. Am. 65 (No. 5), 1073–1095.

Kirkpatrick, J.D., Shipton, Z.K., Persano, C., 2009. Pseudotachylytes: rarely generated, rarely preserved, or rarely reported? Bull. Seismol. Soc. Am. 99 (No. 1). doi:10.1785/0120080114.

Lachenbruch, A.H., 1980. Frictional heating, fluid pressure, and the resistance to fault motion. J. Geophys. Res. 85, 6097–6122.

Mai, P.M., Sommerville, P., Pitarka, A., Dalguer, L., Song, S., Beroza, G., Miyake, H., Irikura, K., 2006. On scaling of fracture energy and stress drop in dynamic rupture models. Consequences for near-source ground-motions. Earthquakes: Radiated Energy and the Physics of Faulting, Geophysical Monograph Series, 170, pp. 283–293. doi:10.1029/170GM24. AGU.

Matsu'ura, M., Kataoka, H., Shibazaki, B., 1992. Slip-dependent friction law and nucleation processes in earthquake rupture. Tectonophys. 211, 135–148.

Mizoguchi, K., Hirose, T., Shimamoto, T., Fukuyama, E., 2009. Fault heals rapidly after dynamic weakening. Bull. Seismol. Soc. Am. 99 (6), 3470–3473. doi:10.1785/0120080325.

Nielsen, S., Di Toro, G., Hirose, T., Shimamoto, T., 2008. Frictional melt and seismic slip. J. Geophys. Res. 113. doi:10.1029/2007JB005122 B01308.

Noda, H., Dunham, E.M., Rice, J.R., 2009. Earthquake ruptures with thermal weakening and the operation of major faults at low overall stress levels. J. Geophys. Res. 114. doi:10.1029/2008JB006143 B07302.

Ohnaka, M., Yamashita, T., 1989. A cohesive zone model for dynamic shear faulting based on experimentally inferred constitutive relation and strong motion source parameters. J. Geophys. Res. 94 (No. B4), 4089–4104.

Okubo, P.G., 1989. Dynamic rupture modeling with laboratory-derived constitutive relations. J. Geophys. Res. 94 (No. B9), 12321–12335.

Rempel, A., Rice, J., 2006. Thermal pressurization and on set of melting in fault zones. J. Geophys. Res. 111. doi:10.1029/2006JB004314 B09314.

Rice, J.R., 2006. Heating and weakening of faults during earthquake slip. J. Geophys. Res. 111 (No. B5). doi:10.1029/2005JB004006 B05311.

Ruina, A.L., 1983. Slip instability and state variable friction laws. J. Geophys. Res. 88 (No. B12), 10359–10370.

Sibson, R.H., 1973. Interaction between temperature and pore-fluid pressure during earthquake faulting — A mechanism for partial or total stress relief. Nature 243, 66–68.

Sibson, R.H., 2003. Thickness of the seismic slip zone. Bull. Seismol. Soc. Am. 93 (No. 3), 1169–1178.

Sleep, N.H., 1997. Application of a unified rate and state friction theory to the mechanics of fault zones with strain localization. J. Geophys. Res. 102 (No. B2), 2875–2895.

Sone, H., Shimamoto, T., 2009. Frictional resistance of faults during accelerating and decelerating earthquake slip. Nature Geosci. doi:10.1038/NGEO637.

Spudich, P., Guatteri, M., Otsuki, K., Minagawa, J., 1998. Use of fault striations and dislocation models to infer tectonic shear stress during the 1995 Hyogo-ken Nanbu (Kobe), Japan, earthquake. Bull. Seismol. Soc. Am. 88, 413–427.

Tinti, E., Bizzarri, A., Piatanesi, A., Cocco, M., 2004. Estimates of slip weakening distance for different dynamic rupture models. Geophys. Res. Lett. 31. doi:10.1029/2003GL018811 L02611.